QUANTUM GASES

Ultrafast many-body interferometry of impurities coupled to a Fermi sea

Marko Cetina,[1,2]* Michael Jag,[1,2] Rianne S. Lous,[1,2] Isabella Fritsche,[1,2] Jook T. M. Walraven,[1,3] Rudolf Grimm,[1,2]† Jesper Levinsen,[4] Meera M. Parish,[4] Richard Schmidt,[5,6] Michael Knap,[7] Eugene Demler[6]

The fastest possible collective response of a quantum many-body system is related to its excitations at the highest possible energy. In condensed matter systems, the time scale for such "ultrafast" processes is typically set by the Fermi energy. Taking advantage of fast and precise control of interactions between ultracold atoms, we observed nonequilibrium dynamics of impurities coupled to an atomic Fermi sea. Our interferometric measurements track the nonperturbative quantum evolution of a fermionic many-body system, revealing in real time the formation dynamics of quasi-particles and the quantum interference between attractive and repulsive states throughout the full depth of the Fermi sea. Ultrafast time-domain methods applied to strongly interacting quantum gases enable the study of the dynamics of quantum matter under extreme nonequilibrium conditions.

The nonequilibrium dynamics of fermionic systems is at the heart of many problems in science and technology. The wide range of energy scales, spanning the low energies of excitations near the Fermi surface up to high energies of excitations from deep within the Fermi sea, challenges our understanding of the quantum dynamics in such fundamental systems. The Fermi energy E_F sets the shortest response time for the collective response of a fermionic many-body system through the Fermi time $\tau_F = \hbar/E_F$, where $\hbar$ is the Planck constant divided by 2π. In a metal (i.e., a Fermi sea of electrons), E_F is in the range of a few electron volts, which corresponds to τ_F on the order of 100 attoseconds. Dynamics in condensed matter systems on this time scale can be recorded by attosecond streaking techniques (*1*), and the initial applications were demonstrated by probing photoelectron emission from a surface (*2*). However, despite these advances, the direct observation of the coherent evolution of a fermionic many-body system on the Fermi time scale has remained beyond reach.

In atomic quantum gases, the fermions are much heavier and the densities far lower, which brings τ_F into the experimentally accessible range of typically a few microseconds. Furthermore, the powerful techniques of atom interferometry (*3*) now offer an opportunity to probe and manipulate the real-time coherent evolution of a fermionic quantum many-body system. Such techniques have been successfully used to measure bosonic Hanbury-Brown-Twiss correlations (*4*), to demonstrate topological bands (*5*), to probe quantum and thermal fluctuations in low-dimensional condensates (*6*, *7*), and to measure demagnetization dynamics of a fermionic gas (*8*, *9*). Impurities coupled to a quantum gas provide a unique probe of the many-body state (*10*–*16*). Strikingly, they allow direct access to the system's wave function when the internal states of the impurities are manipulated using a Ramsey atom-interferometric technique (*17*, *18*).

We used dilute ^{40}K atoms in a ^{6}Li Fermi sea to measure the response of the sea to a suddenly introduced impurity. For near-resonant interactions, we observed coherent quantum many-body dynamics involving the entire ^{6}Li Fermi sea. We also observed in real time the formation dynamics of the repulsive and attractive impurity quasiparticles. In the limit of low impurity concentration, our experiments confirm that an elementary Ramsey sequence is equivalent to linear-response frequency-domain spectroscopy. We demonstrate that our time-domain approaches allow us to prepare, control, and measure many-body interacting states.

Our system consists of a small sample of typically 1.5×10^4 ^{40}K impurity atoms immersed in a Fermi sea of 3×10^5 ^{6}Li atoms (*19*, *20*). The mixture is held in an optical dipole trap (Fig. 1A) at a temperature of $T = 430$ nK after forced evaporative cooling. Because of the Li Fermi pressure, and because our optical potential for K has more than twice the strength of that for Li, the K impurities are concentrated in the central region of the large Li cloud. Here they experience a nearly homogeneous environment with an effective Fermi energy of $\varepsilon_F = k_B \times 2.6$ μK (*20*), where k_B is the Boltzmann constant. The corresponding Fermi time, $\tau_F = 2.9$ μs, sets the natural time scale for our experiments. The degeneracy of the Fermi sea is characterized by $k_B T/\varepsilon_F \approx 0.17$. The concentration of K in the Li sea remains low, with $\overline{n}_K/\overline{n}_{Li} \approx 0.2$, where $\overline{n}_{Li}$ is the average Li number density and $\overline{n}_K$ is the average K number density sampled by the K atoms (*20*).

The interaction between the impurity atoms in the internal state K|3⟩ (third-to-lowest Zeeman sublevel) and the Li atoms (always kept in the

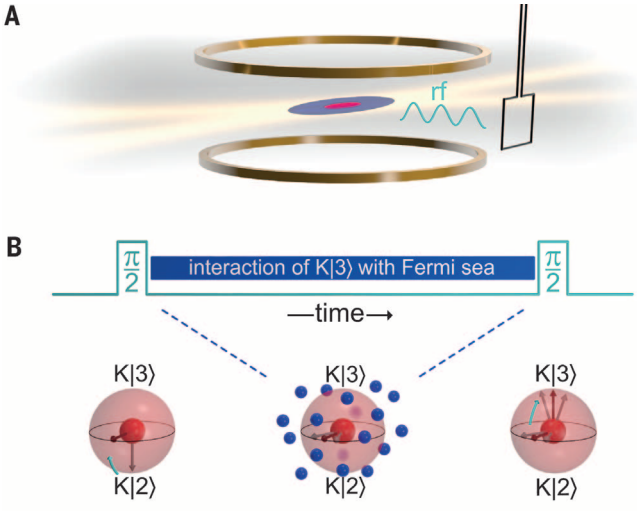

Fig. 1. Illustration of the experimental setup and procedure. (**A**) Li (blue) and K (red) atoms are held in a crossed-beam optical dipole trap, forming the Fermi sea and the sample of impurity atoms, respectively. The magnetic field coils (gold) are used to tune interactions via a Feshbach resonance, and the rf coil (black) allows the manipulation of the spin state of the impurity atoms. (**B**) The Ramsey sequence starts with a first rf $\pi/2$ pulse, which is applied in the presence of weak interactions between the impurity atoms and the Fermi sea. As illustrated on the Bloch sphere, this pulse drives an impurity atom (red dot) into a superposition of the spin states K|2⟩ and K|3⟩. By optical resonance shifting (see text), the interaction of the K|3⟩ component with the atoms of the Fermi sea (blue dots) is abruptly turned on while the K|2⟩ component remains noninteracting. The impurity state then evolves for a variable interaction time, at the end of which its state is probed by a second $\pi/2$ pulse and subsequent measurement of the spin-state populations.

[1]Institut für Quantenoptik und Quanteninformation, Österreichische Akademie der Wissenschaften, 6020 Innsbruck, Austria. [2]Institut für Experimentalphysik, Universität Innsbruck, 6020 Innsbruck, Austria. [3]Van der Waals–Zeeman Institute, Institute of Physics, University of Amsterdam, 1098 XH Amsterdam, Netherlands. [4]School of Physics and Astronomy, Monash University, Victoria 3800, Australia. [5]Institute for Theoretical Atomic, Molecular and Optical Physics (ITAMP), Harvard-Smithsonian Center for Astrophysics, Cambridge, MA 02138, USA. [6]Department of Physics, Harvard University, Cambridge, MA 02138, USA. [7]Department of Physics, Walter Schottky Institute and Institute for Advanced Study, Technical University of Munich, 85748 Garching, Germany.
*Present address: University of Maryland, College Park, MD 20740, USA. †Corresponding author. Email: rudolf.grimm@uibk.ac.at

lowest Zeeman sublevel) is controlled using a rather narrow (*20*) interspecies Feshbach resonance near a magnetic field of 154.7 G (*19*, *21*). We quantify the interaction with the Fermi sea by the dimensionless parameter $X \equiv -1/\kappa_F a$, where $\kappa_F = \hbar^{-1}\sqrt{2m_{Li}\varepsilon_F}$ is the Li Fermi wave number (with m_{Li} the Li mass) and a is the s-wave interspecies scattering length. Slow control of X is realized in a standard way by variations of the magnetic field, whereas fast control is achieved using an optical resonance shifting technique (*19*). The latter permits sudden changes of X by up to ±5 within $\tau_F/15 \approx 200$ ns.

Our interferometric probing method is based on a two-pulse Ramsey scheme (Fig. 1B), following the suggestions of (*17*, *18*). The sequence starts with the impurity atoms prepared in the spin state K|2⟩ (second-to-lowest Zeeman sublevel), for which the background interaction with the Fermi sea can be neglected. An initial radio-frequency (rf) $\pi/2$ pulse, of duration 10 μs, drives the K atoms into a coherent superposition between this noninteracting initial state and the state K|3⟩ under weakly interacting conditions (interaction parameter X_1 with $|X_1| \approx 5$). Using the optical resonance shifting technique (*19*), the system is then rapidly quenched into the strongly interacting regime ($|X| < 1$). After an evolution time t, the system is quenched back into the regime of weak interactions and a second $\pi/2$ pulse is applied. The population difference $N_3 - N_2$ in the two impurity states is measured as a function of the phase ϕ of the rf pulse. By fitting a sine curve to the resulting signal $(N_3 - N_2)/(N_3 + N_2)$, we obtain the contrast $|S(t)|$ and the phase $\varphi(t)$ (*20*), which yields the complex-valued Ramsey signal $S(t) = |S(t)| \exp[-i\varphi(t)]$. In the limit of low impurity concentration and rapid quenching, $S(t) = \langle \exp(i\hat{H}_0 t/\hbar)\exp(-i\hat{H}t/\hbar)\rangle$ describes the sensitivity of the time evolution to perturbations of the system. Here, the angle brackets denote the quantum statistical average, the Hamiltonian $\hat{H}_0$ describes the noninteracting Fermi gas, and the interacting Hamiltonian $\hat{H}$ differs from $\hat{H}_0$ by the additional scattering between the Fermi sea atoms and the impurity atoms. The function $S(t)$, which for pure initial states is often referred to as the Loschmidt amplitude (*22*), was introduced in the context of nuclear magnetic resonance experiments (*23*) and was also applied in the analysis of the orthogonality catastrophe (*24*) as well as in the study of quantum chaos (*25*).

We first consider the interaction conditions for which earlier experiments have demonstrated that the spectral response is dominated by polaronic quasi-particles (*15*). Figure 2, A to D, shows the evolution of the contrast and the phase measured in the repulsive and the attractive polaron regimes, where $X = -0.23 \pm 0.06$ and $X = 0.86 \pm 0.06$, respectively. For short evolution times up to ~4 τ_F, we observed that both contrast signals exhibit a similar initial parabolic transient, which is typical of a Loschmidt echo (*25*). For longer times, this connects to an exponential decay of the contrast and a linear evolution of the phase. In (*19*), we showed that the exponential decay of the contrast in this regime can be interpreted in terms of quasiparticle scattering. Here, the linear phase evolution corresponds to the energy shift of the quasiparticle state, for which we obtain $(+0.29 \pm 0.01)\ \varepsilon_F$ for the repulsive case in Fig. 2C and $(-0.27 \pm 0.01)\ \varepsilon_F$ for the attractive case in Fig. 2D. The longer-time behavior reflects the quasiparticle properties, whereas the observed initial parabolic transient reveals the ultrafast real-time dynamics of the quasiparticle formation.

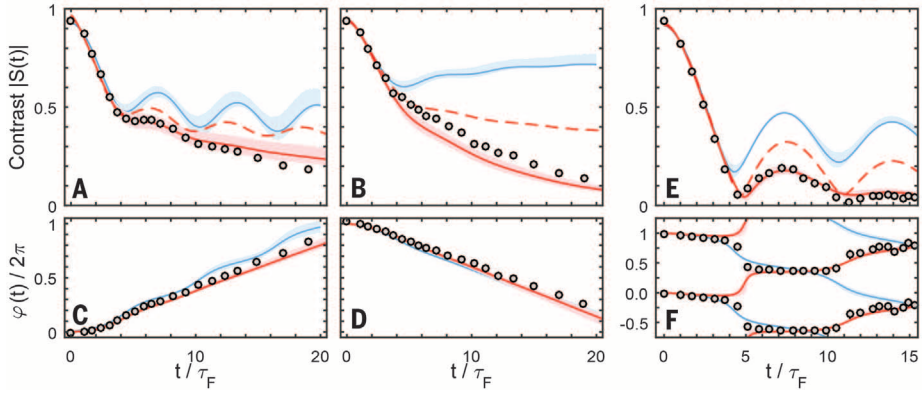

Fig. 2. Impurity dynamics in the Fermi sea. (**A** and **C**) Contrast $|S(t)|$ and phase $\varphi(t)$ of the interference signal depending on the interaction time t in the repulsive polaron regime for $X = -0.23 \pm 0.06$, with the rf pulse applied at $X_1 = -3.9$. (**B** and **D**) Same quantities in the attractive polaron regime for $X = 0.86 \pm 0.06$ and $X_1 = 5.8$. (**E** and **F**) Same quantities for resonant interactions ($X = 0.08 \pm 0.05$, $X_1 = 4.8$). The solid blue lines show the results of the TBM calculations. The solid red lines show the results of the FDA calculations at the measured temperature; the dashed red lines show the calculated results at zero temperature. The shaded regions indicate the uncertainty range resulting from the combined experimental errors in X, k_BT, and ε_F. The errors in the experimental data are typically smaller than the symbol size. The multiple representation of $\varphi(t)$ in (F) accounts for the ambiguity of a phase modulo 2π.

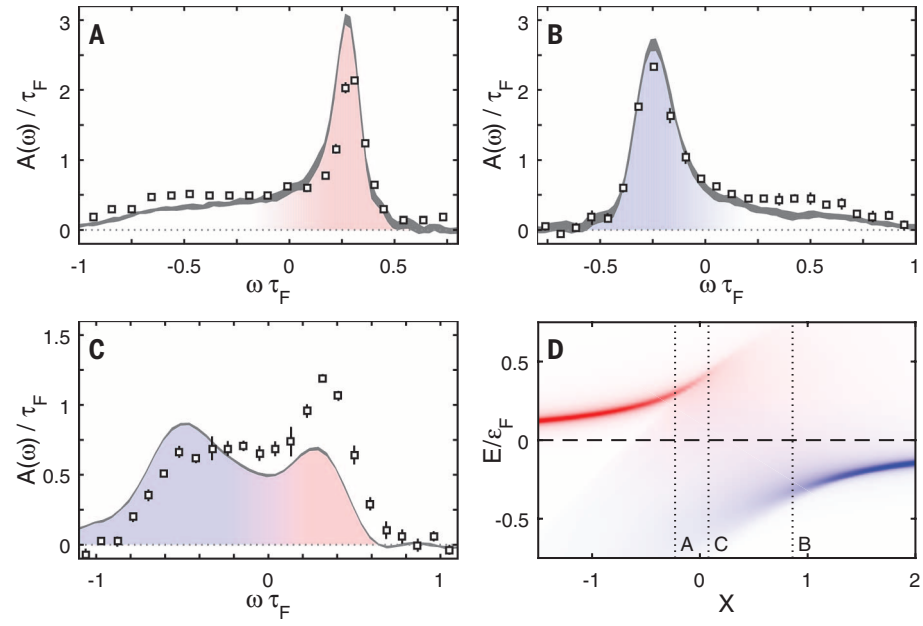

Fig. 3. Frequency-domain rf spectroscopy versus time-domain Ramsey spectroscopy. (**A** to **C**) The data points show the rf spectra for the repulsive ($X = -0.23 \pm 0.06$), attractive ($X = 0.86 \pm 0.06$), and resonant ($X = 0.08 \pm 0.05$) cases, all normalized to unit integral. Here, ω corresponds to the detuning of the rf frequency from the unperturbed transition frequency. The gray lines correspond to the Fourier transform of the $S(t)$ data from Fig. 2, with their widths indicating the standard error resulting from the combined experimental uncertainties in the $S(t)$ data. The red and blue shading indicates the repulsive and attractive parts of the excitation spectrum, respectively. (**D**) Diagram of the excitation energy versus the interaction parameter, showing the repulsive (red) and the attractive (blue) quasiparticle branches. For illustrative purposes, we model the spectrum by a calculation of the spectral function together with additional broadening simulating the effects of finite rf pulse duration and finite temperatures. The three vertical dotted lines indicate the interaction conditions of (A) to (C).

On resonance, for the strongest possible interactions, a description of the dynamics in terms of a single dominant quasiparticle excitation breaks down. In this regime, our measurements—displayed in Fig. 2, E and F, for $X = 0.08 \pm 0.05$—reveal the striking quantum dynamics of an interacting fermionic system forced into a state far out of equilibrium. The contrast $|S(t)|$ shows pronounced oscillations reaching almost zero, which indicates that the time-evolved state can become almost orthogonal to the initial state. Meanwhile, the phase $\varphi(t)$ exhibits plateaus with jumps of π near the contrast minima.

To further interpret our measurements, we used two different theoretical approaches: the truncated basis method (TBM) (*20*) and the functional determinant approach (FDA) (*18*). The TBM models our full experimental procedure assuming zero temperature and considering only single particle-hole excitations. This approximation, first introduced in (*26*) to model the attractive polaron, was later applied to predict repulsive quasi-particles in cold gases (*27*). The predictions of the TBM are represented by the blue lines in Fig. 2. This method accurately describes the initial transient as well as the period of the oscillations of $S(t)$ on resonance. Although the zero-temperature TBM calculation naturally overestimates the contrast in the thermally dominated regime ($t > 6\ \tau_F$), it accurately reproduces the observed linear phase evolution and thus the quasiparticle energy. The FDA is an exact solution for a fixed impurity at arbitrary temperatures, taking into account the nonperturbative creation of infinitely many particle-hole pairs. The FDA calculation is represented by the solid red lines in Fig. 2. We see excellent agreement with our experimental results, which indicates that the effects of impurity motion remain small in our system. This observation can be explained by the fact that our impurity is sufficiently heavy so that the effects of its recoil with energies of ~$0.25\ \varepsilon_F$ (*20*) are masked by thermal fluctuations. To identify the effect of temperature, we performed a corresponding FDA calculation for $T = 0$; the results are shown as dashed lines in Fig. 2. Here, we see a slower decay of $|S(t)|$, which follows a power law at long times (*20*) under the idealizing assumption of infinitely heavy impurities.

Time-domain and frequency-domain methods are closely related, as is well known in spectroscopy. In the limit of low impurity density, where the interactions between the impurities can be neglected, $S(t)$ is predicted to be proportional to the inverse Fourier transform of the linear excitation spectrum $A(\omega)$ of the impurity (*24*). To benchmark our interferometric method, we measured $A(\omega)$ using rf spectroscopy, similar to our earlier work (*12*) but with great care taken to ensure a linear response (*20*). The measured excitation spectra are shown in Fig. 3, A to C, together with a schematic energy diagram of the quasiparticle branches (Fig. 3D). In the repulsive and attractive polaron regimes, we observed the characteristic structure of a peak on top of a broad pedestal (*15*). The peak corresponds to the long-time evolution of the quasiparticle, whereas the pedestal is associated with the rapid dynamics related to the emergence of many-body correlations. For resonant interactions, the rf response is broad and nearly symmetric. The latter implies that the imaginary part of $S(t)$ remains small. Consequently, as seen in Fig. 2, E and F, the phase $\varphi(t)$ essentially takes values near 0 and π, and each phase jump is accompanied by a pronounced minimum of $|S(t)|$.

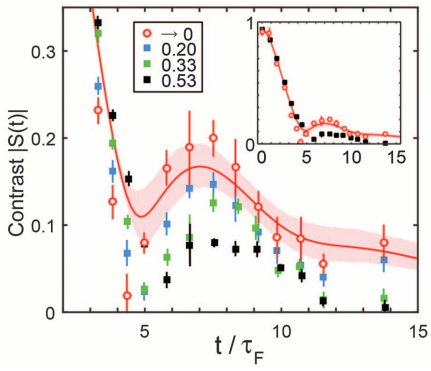

Fig. 4. Observation of induced impurity-impurity interactions. Resonant dynamics of the contrast is shown for $X = -0.01 \pm 0.05$, $X_1 = 5.2$, $\varepsilon_F = k_B \times (2.1 \pm 0.1)$ μK, $k_BT/\varepsilon_F = 0.24 \pm 0.02$, and different impurity concentrations $\overline{n}_K/\overline{n}_{Li}$. The black, green, and blue squares correspond to $\overline{n}_K/\overline{n}_{Li} = 0.53$, 0.33, and 0.20, respectively. The red circles correspond to the linear extrapolation of the complex $S(t)$ data to the limit of a single impurity, taking into account the errors in the data. The inset reproduces this extrapolation together with the highest-concentration data points. The red line shows the result of the FDA calculation, and the shaded region indicates the corresponding uncertainty range resulting from the combined experimental errors in X, k_BT, and ε_F.

The apparent double-hump structure of the spectral response in the resonance regime suggests an interpretation of the observed oscillations of $S(t)$ (Fig. 2E) in terms of a quantum beat between the repulsive and attractive branches of our many-body system. The two branches are strongly broadened and overlap (Fig. 3D), which results in a strong damping of the oscillations.

A detailed comparison of our time- and frequency-domain measurements reveals the potential of our approach to prepare and control many-body states. This is illustrated in Fig. 3, where we show the Fourier transform of the $S(t)$ data from Fig. 2 as gray curves. We observed that time-domain measurements where the rf pulses are applied in the presence of weakly repulsive interactions (Fig. 3A) emphasize the upper branch of the many-body system, whereas in the attractive case (Fig. 3, B and C), the lower branch is emphasized relative to the rf spectra. We interpret this as a consequence of the fact that the residual interactions during the rf pulse already bring the system into a weakly interacting polaron state before it is quenched to resonance (*20*). Relative to the noninteracting initial state used in frequency-domain spectroscopy, these polarons have an increased wave function overlap with the corresponding strongly interacting repulsive and attractive branches, leading to the observed shift in the spectral weight. Our measurements show that the control over the initial state of many particles can be used to manipulate quantum dynamics in the strongly interacting regime. This unique capability of time-domain techniques can potentially be exploited in a wide range of applications, including the study of the dynamical behavior near the phase transition from a polaronic to a molecular system (*15*) and the creation of specific excitations of a Fermi sea down to individual atoms (*28*).

Our interpretation of the results in Figs. 2 and 3 relies on the assumption that our fermionic impurities are sufficiently dilute so that any interactions between them can be neglected. By increasing the impurity concentration, we can extend our experiments into a complex many-body regime where the impurities interact both with the Fermi sea and with each other (*20*). Figure 4 shows the time-dependent contrast measured for $k_BT = 0.24 \pm 0.02\ \varepsilon_F$ and $\overline{n}_K/\overline{n}_{Li} = 0.20$, 0.33, and 0.53. An extrapolation of the $S(t)$ data to zero concentration (open red circles) lies close to the data points for $\overline{n}_K/\overline{n}_{Li} = 0.20$, which is the typical concentration in our measurements and agrees with the FDA calculation. This confirms that the physics that we access in the measurements with a small sample of fermionic impurities is close to that of a single impurity, which we posit to be a consequence of the fermionic nature of the impurities. When the impurity concentration is increased, we find that the contrast for $t > 5\ \tau_F$ is decreased and the period of the revivals of $|S(t)|$ is prolonged. We interpret this as arising from effective interactions between the impurities induced by the Fermi sea (*29*, *30*). Such interactions between fermionic impurities are predicted to lead to interesting quantum phases (*31*).

Our results demonstrate the power of many-body interferometry to study ultrafast processes in strongly interacting Fermi gases in real time, including the formation dynamics of quasi-particles and the nonequilibrium dynamics arising from quantum interference between different many-body branches. Of particular interest is the prospect of observing Anderson's orthogonality catastrophe (*18*, *20*) by further cooling the Li Fermi sea (*32*) while pinning the K atoms in a deep species-selective optical lattice (*33*).

REFERENCES AND NOTES

1. F. Krausz, M. Ivanov, *Rev. Mod. Phys.* **81**, 163–234 (2009).
2. R. Pazourek, S. Nagele, J. Burgdörfer, *Rev. Mod. Phys.* **87**, 765–802 (2015).
3. A. D. Cronin, J. Schmiedmayer, D. E. Pritchard, *Rev. Mod. Phys.* **81**, 1051–1129 (2009).
4. J. Simon *et al.*, *Nature* **472**, 307–312 (2011).
5. M. Atala *et al.*, *Nat. Phys.* **9**, 795–800 (2013).
6. M. Gring *et al.*, *Science* **337**, 1318–1322 (2012).
7. Z. Hadzibabic, P. Krüger, M. Cheneau, B. Battelier, J. Dalibard, *Nature* **441**, 1118–1121 (2006).
8. M. Koschorreck, D. Pertot, E. Vogt, M. Köhl, *Nat. Phys.* **9**, 405–409 (2013).
9. A. B. Bardon *et al.*, *Science* **344**, 722–724 (2014).

10. A. Schirotzek, C.-H. Wu, A. Sommer, M. W. Zwierlein, *Phys. Rev. Lett.* **102**, 230402 (2009).
11. S. Nascimbène *et al.*, *Phys. Rev. Lett.* **103**, 170402 (2009).
12. C. Kohstall *et al.*, *Nature* **485**, 615–618 (2012).
13. M. Koschorreck *et al.*, *Nature* **485**, 619–622 (2012).
14. Y. Zhang, W. Ong, I. Arakelyan, J. E. Thomas, *Phys. Rev. Lett.* **108**, 235302 (2012).
15. P. Massignan, M. Zaccanti, G. M. Bruun, *Rep. Prog. Phys.* **77**, 034401 (2014).
16. M. Sidler *et al.*, http://arXiv.org/abs/1603.09215 (2016).
17. J. Goold, T. Fogarty, N. Lo Gullo, M. Paternostro, T. Busch, *Phys. Rev. A* **84**, 063632 (2011).
18. M. Knap *et al.*, *Phys. Rev. X* **2**, 041020 (2012).
19. M. Cetina *et al.*, *Phys. Rev. Lett.* **115**, 135302 (2015).
20. See supplementary materials on *Science* Online.
21. D. Naik *et al.*, *Eur. Phys. J. D* **65**, 55–65 (2011).
22. J. Loschmidt, *Sitzungsber. Akad. Wissenschaften Wien* **73**, 128 (1876).
23. E. L. Hahn, *Phys. Rev.* **80**, 580–594 (1950).
24. P. Nozières, C. T. De Dominicis, *Phys. Rev.* **178**, 1097–1107 (1969).
25. R. A. Jalabert, H. M. Pastawski, *Adv. Solid State Phys.* **41**, 483–496 (2001).
26. F. Chevy, *Phys. Rev. A* **74**, 063628 (2006).
27. X. Cui, H. Zhai, *Phys. Rev. A* **81**, 041602 (2010).
28. J. Dubois *et al.*, *Nature* **502**, 659–663 (2013).
29. C. Mora, F. Chevy, *Phys. Rev. Lett.* **104**, 230402 (2010).
30. Z. Yu, S. Zöllner, C. J. Pethick, *Phys. Rev. Lett.* **105**, 188901 (2010).
31. W. Zwerger, Ed., *The BCS-BEC Crossover and the Unitary Fermi Gas* (Springer, 2012).
32. R. A. Hart *et al.*, *Nature* **519**, 211–214 (2015).
33. L. J. LeBlanc, J. H. Thywissen, *Phys. Rev. A* **75**, 053612 (2007).

ACKNOWLEDGMENTS

We thank M. Baranov, F. Schreck, G. Bruun, N. Davidson, and R. Folman for stimulating discussions. Supported by NSF through a grant for ITAMP at Harvard University and the Smithsonian Astrophysical Observatory (R.S.); the Technical University of Munich-Institute for Advanced Study, funded by the German Excellence Initiative and the European Union FP7 under grant agreement 291763 (M.K.); the Harvard-MIT Center for Ultracold Atoms, NSF grant DMR-1308435, the Air Force Office of Scientific Research Quantum Simulation Multidisciplinary University Research Initiative (MURI), the Army Research Office MURI on Atomtronics, M. Rössler, the Walter Haefner Foundation, the ETH Foundation, and the Simons Foundation (E.D.); and the Austrian Science Fund (FWF) within the SFB FoQuS (F4004-N23) and within the DK ALM (W1259-N27).

SUPPLEMENTARY MATERIALS

www.sciencemag.org/content/354/6308/96/suppl/DC1
Materials and Methods
Supplementary Text
Figs. S1 to S11
Table S1
References (*34*–*56*)

20 February 2016; accepted 6 September 2016
10.1126/science.aaf5134

DEVICE TECHNOLOGY

MoS_2 transistors with 1-nanometer gate lengths

Sujay B. Desai,[1,2,3] Surabhi R. Madhvapathy,[1,2] Angada B. Sachid,[1,2] Juan Pablo Llinas,[1,2] Qingxiao Wang,[4] Geun Ho Ahn,[1,2] Gregory Pitner,[5] Moon J. Kim,[4] Jeffrey Bokor,[1,2] Chenming Hu,[1] H.-S. Philip Wong,[5] Ali Javey[1,2,3]*

Scaling of silicon (Si) transistors is predicted to fail below 5-nanometer (nm) gate lengths because of severe short channel effects. As an alternative to Si, certain layered semiconductors are attractive for their atomically uniform thickness down to a monolayer, lower dielectric constants, larger band gaps, and heavier carrier effective mass. Here, we demonstrate molybdenum disulfide (MoS_2) transistors with a 1-nm physical gate length using a single-walled carbon nanotube as the gate electrode. These ultrashort devices exhibit excellent switching characteristics with near ideal subthreshold swing of ~65 millivolts per decade and an On/Off current ratio of ~10^6. Simulations show an effective channel length of ~3.9 nm in the Off state and ~1 nm in the On state.

As Si transistors rapidly approach their projected scaling limit of ~5-nm gate lengths, exploration of new channel materials and device architectures is of utmost interest (*1*–*3*). This scaling limit arises from short channel effects (*4*). Direct source-to-drain tunneling and the loss of gate electrostatic control on the channel severely degrade the Off state leakage currents, thus limiting the scaling of Si transistors (*5*, *6*). Certain semiconductor properties dictate the magnitude of these effects for a given gate length. Heavier carrier effective mass, larger band gap, and lower in-plane dielectric constant yield lower direct source-to-drain tunneling currents (*7*). Uniform and atomically thin semiconductors with low in-plane dielectric constants are desirable for enhanced electrostatic control of the gate. Thus, investigation and introduction of semiconductors that have more ideal properties than Si could lead to further scaling of transistor dimensions with lower Off state dissipation power.

Transition metal dichalcogenides (TMDs) are layered two-dimensional (2D) semiconductors that have been widely explored as a potential channel material replacement for Si (*8*–*11*), and each material exhibits different band structures and properties (*12*–*16*). The layered nature of TMDs allows uniform thickness control with atomic-level precision down to the monolayer limit. This thickness scaling feature of TMDs is highly desirable for well-controlled electrostatics in ultrashort transistors (*3*). For example, monolayer and few-layer MoS_2 have been shown theoretically to be superior to Si at the sub-5-nm scaling limit (*17*, *18*).

The scaling characteristics of MoS_2 and Si transistors as a function of channel thickness and gate length are summarized in Fig. 1. We calculated direct source-to-drain tunneling currents ($I_{SD\text{-}LEAK}$) in the Off state for different channel lengths and thicknesses using a dual-gate device structure (fig. S1) as a means to compare the two materials. MoS_2 shows more than two orders of magnitude reduction in $I_{SD\text{-}LEAK}$ relative to Si mainly because of its larger electron effective mass along the transport direction ($m_n^* \sim 0.55m_0$ for MoS_2 versus $m_n^* \sim 0.19m_0$ for Si [100]) (*19*), with a trade-off resulting in lower ballistic On current. Notably, $I_{SD\text{-}LEAK}$ does not limit the scaling of monolayer MoS_2 even down to the ~1-nm gate length, presenting a major advantage over Si [see more details about calculations in the supplementary materials (*20*)]. Finally, few-layer MoS_2 exhibits a lower in-plane dielectric constant (~4) compared with bulk Si (~11.7), Ge (~16.2), and GaAs (~12.9), resulting in a shorter electrostatic characteristic length (λ) as depicted in fig. S2 (*21*).

The above qualities collectively make MoS_2 a strong candidate for the channel material of future transistors at the sub-5-nm scaling limit. However, to date, TMD transistors at such small gate lengths have not been experimentally explored. Here, we demonstrate 1D gated, 2D semiconductor field-effect transistors (1D2D-FETs) with a single-walled carbon nanotube (SWCNT) gate, a MoS_2 channel, and physical gate lengths of ~1 nm. The 1D2D-FETs exhibit near ideal switching characteristics, including a subthreshold swing (SS) of ~65 mV per decade at room temperature and high On/Off current ratios. The SWCNT diameter $d \sim 1$ nm for the gate electrode (*22*) minimized parasitic gate to source-drain capacitance, which is characteristic of lithographically patterned tall gate structures. The ~1-nm gate length of the SWCNT also allowed for the experimental exploration of the device physics and properties of MoS_2 transistors as a function of semiconductor thickness (i.e., number of layers) at the ultimate gate-length scaling limit.

The experimental device structure of the 1D2D-FET (Fig. 2A) consists of a MoS_2 channel (number of layers vary), a ZrO_2 gate dielectric, and a SWCNT gate on a 50-nm SiO_2/Si substrate with a physical gate length ($L_G \sim d$) of ~1 nm. Long, aligned SWCNTs grown by chemical vapor deposition

[1]Electrical Engineering and Computer Sciences, University of California, Berkeley, CA 94720, USA. [2]Materials Sciences Division, Lawrence Berkeley National Laboratory, Berkeley, CA 94720, USA. [3]Berkeley Sensor and Actuator Center, University of California, Berkeley, CA 94720, USA. [4]Department of Materials Science and Engineering, University of Texas at Dallas, Richardson, TX 75080, USA. [5]Electrical Engineering, Stanford University, Stanford, CA 94305, USA.
***Corresponding author. Email: ajavey@eecs.berkeley.edu**

Ultrafast many-body interferometry of impurities coupled to a Fermi sea

Marko Cetina, Michael Jag, Rianne S. Lous, Isabella Fritsche, Jook T. M. Walraven, Rudolf Grimm, Jesper Levinsen, Meera M. Parish, Richard Schmidt, Michael Knap and Eugene Demler

Science **354** (6308), 96-99.
DOI: 10.1126/science.aaf5134

Sluggish turmoil in the Fermi sea

The nonequilibrium dynamics of many-body quantum systems are tricky to study experimentally or theoretically. As an experimental setting, dilute atomic gases offer an advantage over electrons in metals. In this environment, the heavier atoms make collective processes that involve the entire Fermi sea occur at the sluggish time scale of microseconds. Cetina *et al.* studied these dynamics by using a small cloud of ^{40}K atoms that was positioned at the center of a far larger ^{6}Li cloud. Controlling the interactions between K and Li atoms enabled a detailed look into the formation of quasiparticles associated with K "impurity" atoms.

Science, this issue p. 96